



**Structure of the Polycrystalline Zeolite Catalyst IM-5
Solved by Enhanced Charge Flipping**

Christian Baerlocher, *et al.*
Science **315**, 1113 (2007);
DOI: 10.1126/science.1137920

**The following resources related to this article are available online at
www.sciencemag.org (this information is current as of February 23, 2007):**

Updated information and services, including high-resolution figures, can be found in the online version of this article at:

<http://www.sciencemag.org/cgi/content/full/315/5815/1113>

Supporting Online Material can be found at:

<http://www.sciencemag.org/cgi/content/full/315/5815/1113/DC1>

This article appears in the following **subject collections**:

Chemistry

<http://www.sciencemag.org/cgi/collection/chemistry>

Information about obtaining **reprints** of this article or about obtaining **permission to reproduce this article** in whole or in part can be found at:

<http://www.sciencemag.org/help/about/permissions.dtl>

Structure of the Polycrystalline Zeolite Catalyst IM-5 Solved by Enhanced Charge Flipping

Christian Baerlocher,¹ Fabian Gramm,¹ Lars Massüger,¹ Lynne B. McCusker,^{1*} Zhanbing He,² Sven Hovmöller,² Xiaodong Zou²

Despite substantial advances in crystal structure determination methodology for polycrystalline materials, some problems have remained intractable. A case in point is the zeolite catalyst IM-5, whose structure has eluded determination for almost 10 years. Here we present a charge-flipping structure-solution algorithm, extended to facilitate the combined use of powder diffraction and electron microscopy data. With this algorithm, we have elucidated the complex structure of IM-5, with 24 topologically distinct silicon atoms and an unusual two-dimensional medium-pore channel system. This powerful approach to structure solution can be applied without modification to any type of polycrystalline material (e.g., catalysts, ceramics, pharmaceuticals, complex metal alloys) and is therefore pertinent to a diverse range of scientific disciplines.

As a result of impressive methodological advances in recent years, the determination of a crystal structure from powder diffraction data is no longer a rarity (1, 2). However, some problems have remained intractable. The prospect of dealing successfully with such cases has been improved recently by two developments. First, the charge-flipping structure-solution algorithm introduced by Oszlányi and Sütő in 2004 for single-crystal data (3, 4) has been adapted to accommodate powder diffraction data (5). The resulting powder charge-flipping (pCF) algorithm implemented in the program Superflip (6) has been shown to work well with both organic and inorganic materials of varying complexities. The second advance involves the inclusion of crystallographic phases obtained from high-resolution transmission electron microscopy (HRTEM) images in the input to the zeolite-specific program FOCUS (7). This approach led to the solution of the extremely complex structure of the polycrystalline zeolite TNU-9 (8). We reasoned that by including crystallographic phases from HRTEM images in the pCF algorithm, a powerful and generally applicable approach to structure solution for polycrystalline materials could be developed. We were particularly eager to apply this method to the polycrystalline zeolite catalyst IM-5, whose structure has eluded determination for almost 10 years.

The synthesis of the high-silica zeolite IM-5 was reported in 1998 (9), and the general features of its pore system were deduced from catalytic test reactions in 2000 (10). Although the material has proven to be an important thermally stable catalyst for hydrocarbon cracking and NO reduction (11–16), its properties cannot be fully

understood without detailed crystal structure information. Like many zeolitic materials, IM-5 is polycrystalline, but this alone does not account for the particular challenge posed by its structure analysis. It has an unusually large unit cell (*C*-centered orthorhombic with $a = 14.299 \text{ \AA}$, $b = 57.413 \text{ \AA}$, and $c = 20.143 \text{ \AA}$) with a volume almost triple that of ZSM-5 (17), one of the more complex known zeolites. There are also approximate relationships between the axes ($b \sim 4a$ and $c \sim \sqrt{2}a$), which means that symmetrically unrelated reflections (e.g., 200 and 080 or 022 and 060) have very similar d spacings. These factors result in an enormous degree of reflection overlap, which is the key hindrance to structure solution from powder diffraction data (1). Furthermore, impurities, which complicate any powder diffraction data analysis, are common in IM-5 syntheses. We overcame these difficulties by combining powder diffraction and electron microscopy techniques in a charge-flipping structure-solution algorithm.

This study builds on our prior adaptation of the charge-flipping algorithm to accommodate powder diffraction data (5). The algorithm itself is a deceptively simple one. Structure factor amplitudes ($|F_{hkl}|$), derived from the measured diffraction intensities (I_{hkl}), are assigned random crystallographic phases (ϕ_{hkl}), and the corresponding (random) electron density map [$\rho(xyz)$] is generated with the equation

$$\rho(xyz) = \frac{1}{V} \sum_{hkl} |F_{hkl}| \cos(2\pi(hx + ky + lz) - \phi_{hkl}) \quad (1)$$

Then the signs of all electron density pixels below a user-defined threshold value δ (a small positive number close to zero) are reversed (hence “charge flipping”) to produce a modified electron density map. Essentially, all negative electron densities (which are not physically meaningful) are made positive. From this map, a new set of structure factor amplitudes and phases is calculated. The new phases are then

combined with the measured amplitudes to produce a new electron density map. This cycle is repeated until convergence (calculated amplitudes matching measured ones) is reached. An R value comparing the calculated and measured amplitudes provides an estimate of the reliability of the final map.

In a powder diffraction pattern, reflections with similar d spacings (or diffraction angle 2θ) overlap, obscuring their individual intensities. To improve the initial estimate of these intensities (usually a simple equipartitioning) during the course of a pCF run, we introduced a periodic repartitioning within each overlap group. In our implementation, this repartitioning procedure involves an additional density modification based on histogram matching (18) and is performed after a user-defined number of cycles of charge flipping. Wu and co-workers use the charge-flipping modification itself for this repartitioning step (19). The advantages of the charge-flipping algorithm are twofold. First, all calculations are performed without any assumptions about the symmetry, thereby side-stepping space group ambiguities, common in powder diffraction data. Second, no chemical information (e.g., bond distances, bond angles, atom connectivity) is required, so the technique can be applied to any class of material. The question was whether or not this algorithm could handle a problem as complex as the structure of IM-5.

In parallel to the development of the pCF algorithm, we were exploring ways of combining the complementary aspects of powder diffraction and electron microscopy techniques for structure determination. In the case of TNU-9 (8) mentioned earlier, intensities extracted from high-resolution powder diffraction data were combined with crystallographic phases obtained from HRTEM images in the zeolite-specific program FOCUS (7). We reasoned that a similar approach could be used for IM-5, except that the information from the two techniques would be combined in the pCF algorithm rather than in FOCUS. Because the pCF algorithm operates in both real (electron density) and reciprocal (phase) space, it is relatively easy to add supplementary information in either realm. For example, a partial or approximate model can be introduced in real space as a starting electron density map, instead of the usual random phase map; a (partial) pore system in a zeolite can be defined in real space in terms of a structure envelope (20); or phase information from HRTEM images can be added in reciprocal space.

High-resolution powder diffraction data were collected from several different samples of IM-5 at the Swiss-Norwegian Beamlines (SNBL) at the European Synchrotron Radiation Facility in Grenoble, France, and the Swiss Light Source (SLS) in Villigen. None of the samples were ideal. All contained impurities, none had particularly sharp peaks, and diffraction intensity decreased rapidly with diffraction angle. Indeed, the main difference between IM-5 and TNU-9 in

¹Laboratory of Crystallography, ETH Zurich, CH-8093 Zurich, Switzerland. ²Structural Chemistry, Stockholm University, SE-106 91 Stockholm, Sweden.

*To whom correspondence should be addressed. E-mail: mccusker@mat.ethz.ch

terms of the difficulty of the structure determination lies in the inferior quality of the IM-5 powder diffraction data. Nonetheless, by comparing the different IM-5 patterns, the peaks corresponding to the IM-5 phase could be distinguished from those of the various impurities, and a tentative indexing of the patterns achieved. In some patterns, the impurity peaks could be assigned to known materials, but in others they remained unidentified. Because of the relationships between the axes mentioned earlier and the quality of the data, the indexing was uncertain and the cell difficult to refine. Generally, determining the unit cell from a powder diffraction pattern is a straightforward and accurate procedure. How-

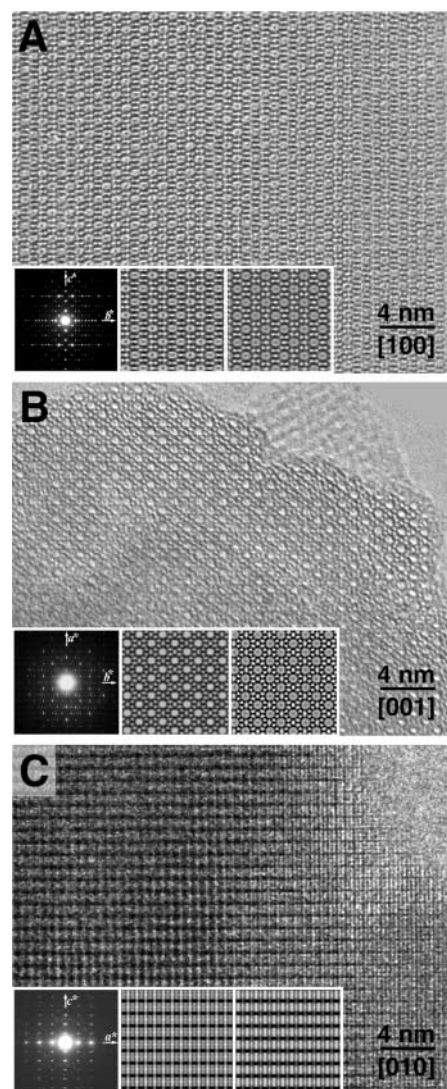


Fig. 1. HRTEM images taken along different zone axes of IM-5. (A) [100], (B) [001], and (C) [010]. Insets show the corresponding selected-area electron diffraction patterns (left), the symmetry-averaged images (middle), and the simulated images from the structural model (right). The crystal thicknesses for the simulations were 50, 50, and 750 Å, and the defocus values were -500, -400, and +1500 Å, respectively.

ever, when reflection overlap is extreme and/or when unidentified impurities are present, electron diffraction is a valuable complementary technique. Because electrons interact much more strongly with atoms than do x-rays, a single-crystal electron diffraction pattern can be obtained from a very tiny crystallite (dimensions of ~20 nm versus ~20 μm for x-rays). Unfortunately, this strong interaction generally results in intensities that are difficult or impossible to interpret directly. However, the single-crystal nature of the diffraction patterns allows impurities to be discriminated from the main phase and reflections with similar d spacings to be distinguished from one another.

We therefore collected series of selected area electron diffraction (SAED) patterns on different crystallites of IM-5 as they were tilted around various axes. The SAED patterns from each tilt series were combined with the programs ELD (21) and Trice (22) to construct a three-dimensional (3D) reciprocal lattice, from which approximate lattice parameters could be determined. These results confirmed the powder indexing. The systematic absences in the SAED patterns indicated that the most probable space groups were $Cmc2_1$, $C2cm$, and $Cmcm$.

The powder diffraction pattern exhibiting the sharpest peaks and the largest range in d spacings (20) was selected for further analysis. First, the analcime impurity peaks were subtracted from this pattern, and then a set of reflection intensities were extracted assuming the space group $Cmcm$. Of the 4120 reflections in the pattern ($d_{\min} = 1.05$ Å), 3499 were within $0.2 \times$ FWHM (full width at half maximum) of another reflection, forming 862 overlap groups. To optimize the relative intensities within the overlap groups, the FIPS (fast iterative Patterson squaring) routine was applied (23). These intensities were expanded to the space group $P1$ (no symmetry within the unit cell) and used as input to the pCF program. Although some of the resulting electron density maps showed feasible pore systems, none could be interpreted to a level sufficient for structure determination. There were indications in these maps that the assignment of a mirror plane perpendicular to the a axis (in $Cmcm$) might be erroneous.

To resolve this issue, we took high-quality HRTEM images of IM-5 along the three main zone axes at 300 kV on a JEM-3010 transmission electron microscope (Fig. 1). A Fourier transform was calculated from a thin area near the crystal edge in each image, and structure factor amplitudes and phases were extracted with the program CRISP (24). Note that crystallographic phases, which are lost in diffraction experiments, can be retrieved from HRTEM images. These phases were analyzed to determine the symmetry of each projection, and the combination of the three different projections supported the assignment of the noncentrosymmetric space group $C2cm$ (standard setting $Ama2$). Consequently, the phase relations and phase restrictions of the space group $C2cm$ were imposed on the amplitudes and phases extracted from the HRTEM images of each projection. The contrast transfer function was determined from the Fourier transform of each image and compensated with the program CRISP, after which the projected potential maps (insets in Fig. 1) were calculated.

The structure factor amplitudes and phases from the three HRTEM projections were combined to produce a 3D set of 95 structure factors. Common reflections were used to scale the amplitudes and to determine the common origin of the different projections (25). A 3D potential map was then calculated by inverse Fourier transformation with the program eMap (26). In this potential map, 36 unique Si-atom positions were located and then adjusted to produce a four-connected framework structure. Oxygen bridges were added between the connected Si atoms, and the geometry was optimized with the distance least-squares program DLS-76 (27). However, the R value of the optimization (comparison of calculated and ideal distances) indicated that the framework was highly strained. Furthermore, the powder diffraction pattern generated from this model did not fit the measured one very well, even after structure refinement.

The 95 phases derived from the HRTEM images were then included in the pCF routine, along with a structure envelope (20) defining the channels along [100] and [001] (Fig. 1, A and B). The structure envelope was used to eliminate electron density within the channels. However,

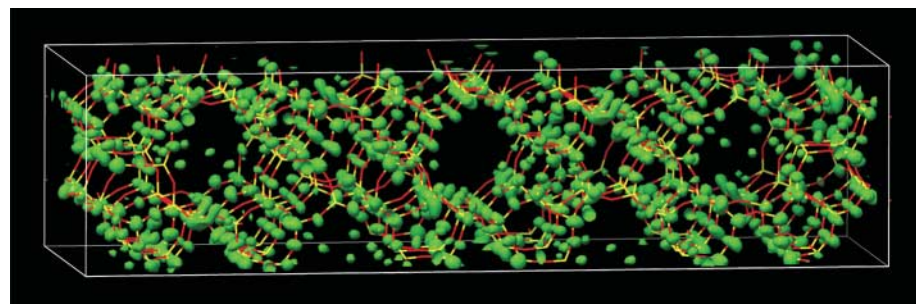


Fig. 2. Electron density map from pCF that was used to derive the structure of IM-5. A stick model of the final refined structure of IM-5 has been superimposed for comparison. The image was produced with the UCSF Chimera package (30).

the resulting electron density maps were not improved sufficiently over the earlier ones for meaningful interpretation. Speculating that the model derived from the HRTEM data was probably partially correct, we used it to calculate alternative starting electron density maps to replace the initial map generated by the use of random phases. The phase of each reflection calculated from the structure was varied by up to

25% in random fashion, thereby generating 1000 different starting points for 1000 distinct pCF runs. During the course of each run, the channel system was enforced periodically by applying the structure envelope restriction. The resulting maps were symmetry averaged assuming the space group $C2cm$, and then the five best maps (lowest pCF R values) were combined to yield the one shown in Fig. 2.

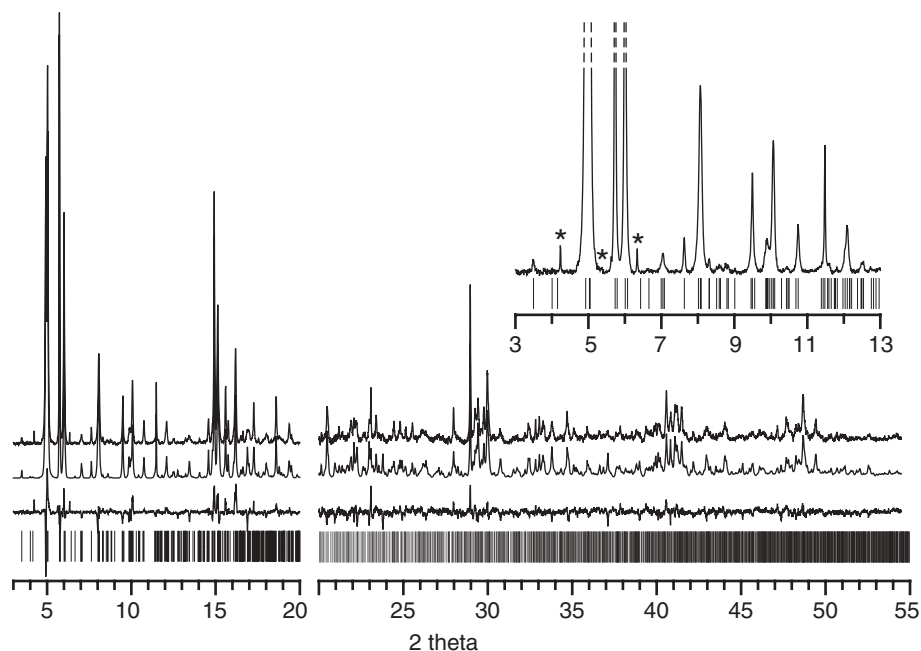


Fig. 3. Observed (top), calculated (middle), and difference (bottom) diffraction profiles for the Rietveld refinement of calcined IM-5 ($\lambda = 0.99995$ Å). The higher-angle data have been scaled up by a factor of 4 to show more detail. Tick marks indicate the positions of the reflections. A small section of the low-angle data has been expanded in the inset to illustrate the high degree of reflection overlap even in the large d -spacing range. Three clearly separated impurity peaks are marked with asterisks.

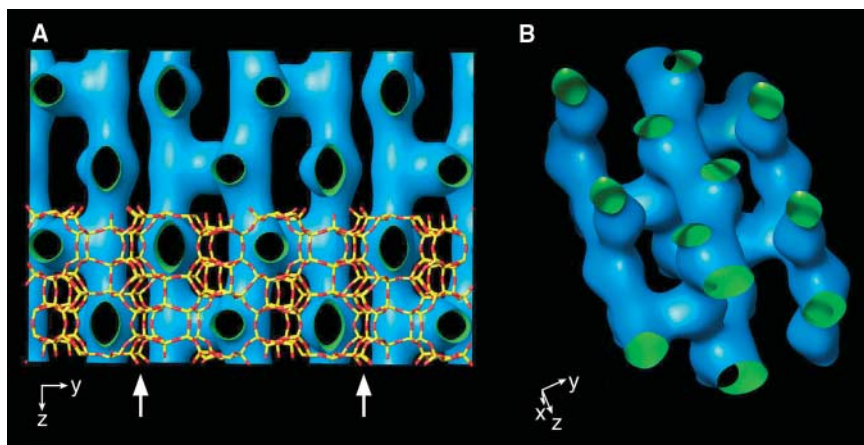


Fig. 4. The unusual 2D 10-ring channel system of IM-5. (A) Projection along [100], showing the connections between the channels running parallel to [001]. The walls between channel systems are marked with arrows. (B) A single 2D channel system [between the walls marked in (A)], showing more detail of the connectivity. The details of the shape and size of the structure envelope (generated from 21 reflections) used to depict the channel system are only approximate and should not be overinterpreted. The envelope is only meant to indicate the approximate arrangement of the channels within the framework structure. The image was produced with the UCSF Chimera package (30).

Interpretation of this map was almost trivial. The positions of 35 of the 36 Si atoms and 61 of the 79 O atoms could be located directly in the top 106 peaks. The position of the missing Si atom could be deduced quite easily from the four surrounding Si atoms. Two of the other Si atoms had to be shifted by ~ 0.1 Å along the c axis to complete the four-connected framework structure. The positions of the missing oxygen bridges were then generated, and the geometry was optimized with DLS-76 (27). This time, the DLS R value was indicative of an unstrained geometry, and the calculated powder diffraction pattern matched the main features of the measured one.

The framework structure appeared to be consistent with the centrosymmetric space group $Cmcm$, so we began Rietveld refinement of the structure assuming this symmetry. To simplify the refinement, we used data collected on a calcined sample (i.e., one in which the organic molecules in the pores had been removed by heat treatment) [$a = 14.2088(3)$ Å, $b = 57.2368(13)$ Å, $c = 19.9940(2)$ Å], even though the peaks were not as sharp as those in the pattern used for the structure determination. Soft geometric restraints were placed on the bond distances and angles of the atoms of the framework, and the refinement converged with the structure factor, weighted profile (R_{wp}), and statistically expected R values 0.075, 0.188, and 0.142, respectively (Fig. 3). Strong anisotropic peak broadening along two crystallographic directions (e.g., peak widths of 0.026, 0.060, and $0.068^\circ 2\theta$ for reflections with similar 2θ values, but orthogonal orientations) was observed and could only be modeled approximately. The high R_{wp} value stems mainly from this complication, as well as a particularly irregular background that was difficult to estimate and the presence of an unidentified impurity. Nonetheless, the refinement of the structure itself was extremely stable. Although 12 of the 24 Si atoms in the asymmetric unit lie on the mirror plane perpendicular to the a axis, the geometry remained reasonable, with the possible exception of the 180° Si-O-Si angle at O(25), which lies on a center of symmetry. Reducing the symmetry to one of the non-centrosymmetric C -centered subgroups of $Cmcm$ ($C2cm$, $C22_1$, or Cmc_1) did not result in any substantial improvement in either the profile fit or the geometry, so the higher space group $Cmcm$ was retained. It is possible that the calcined form of IM-5, which was used for the refinement, adopts a symmetry higher than that of the as-synthesized form, which was used for all the other analyses.

With 24 topologically distinct Si atoms, the framework structure of IM-5 (see data file S1 for IM-5 crystallographic information) is as complex as that of TNU-9, the most complex zeolite hitherto solved (8). For comparison, the next most complex zeolite, ITQ-22 (28), has only 16 topologically distinct (Si,Ge) atoms. The [001]

projection (Fig. 1B) of IM-5 is very similar to one found in several other high-silica zeolites [Ferrierite, ZSM-5, ZSM-11, ZSM-57, SUZ-4, Theta-1, and TNU-9 (29)]. However, the connectivity along [001] is different and leads to an unusual pore system (Fig. 4). As suggested by the catalytic tests (10), IM-5 has a 2D 10-ring (10 Si atoms and 10 O atoms in the ring describing the pore opening) channel system with effective pore widths ranging from 4.8 to 5.5 Å. What is unusual is that this channel system also has a limited third dimension. Three 2D channel systems running perpendicular to the *b* axis are connected to one another to form a ~2.5-nm-thick pore system. Single walls of four, five, and six rings (Fig. 4A) separate these nanoslabs from one another. This distinctive pore structure (Fig. 4B) gives IM-5 the character of a 3D channel system with complex channel intersections that can accommodate bulky intermediates in a catalytic reaction, while retaining the overall effect of a 2D one with long-range diffusion restricted to just two dimensions.

Because no symmetry is assumed, the number of atoms per unit cell rather than the number per asymmetric unit is the prime limitation of the pCF algorithm. For IM-5, this number is 864 (288 Si atoms + 576 O atoms). Therefore, the structures of other polycrystalline materials with similar numbers of atoms per unit cell, whether they be other catalysts, ceramics, pharmaceuticals, or complex metal alloys, should also be accessible via a similar route, provided that

HRTEM images can be obtained. All of the enhancements to the charge-flipping approach discussed here have been implemented in the freely available program Superflip (Superflip input file for IM-5 is given in data file S2) (6).

References and Notes

- W. I. F. David, K. Shankland, L. B. McCusker, Ch. Baerlocher, Eds., *Structure Determination from Powder Diffraction Data* (Oxford Univ. Press, Oxford, 2002).
- Ch. Baerlocher, L. B. McCusker, Eds., *Z. Kristallogr.* **219** (Spec. Iss.), 782 (2004).
- G. Oszlányi, A. Sütő, *Acta Crystallogr. A* **60**, 134 (2004).
- G. Oszlányi, A. Sütő, *Acta Crystallogr. A* **61**, 147 (2005).
- Ch. Baerlocher, L. B. McCusker, L. Palatinus, *Z. Kristallogr.* **222**, 47 (2007).
- L. Palatinus, G. Chapuis, <http://superspace.epfl.ch/superflip> (2006).
- R. W. Grosse-Kunstleve, L. B. McCusker, Ch. Baerlocher, *J. Appl. Cryst.* **30**, 985 (1997).
- F. Gramm *et al.*, *Nature* **444**, 79 (2006).
- E. Benazzi, J. L. Guth, L. Rouleau, *PCT Gazette* WO 98/17581 (1998).
- A. Corma *et al.*, *J. Catal.* **189**, 382 (2000).
- A. Corma, J. Martínez-Triguero, S. Valencia, E. Benazzi, S. Lacombe, *J. Catal.* **206**, 125 (2002).
- S.-H. Lee *et al.*, *J. Catal.* **215**, 151 (2003).
- E. Benazzi, S. Kasztelan, U.S. Patent 6667267 (2003).
- J. M. Serra, E. Guillon, A. Corma, *J. Catal.* **227**, 459 (2004).
- J. M. Serra, E. Guillon, A. Corma, in *Molecular Sieves: From Basic Research to Industrial Applications*, J. Cejka, N. Zilkova, P. Nachtigall, Eds. (Elsevier, Amsterdam, 2005), vol. 158, p. 1757.
- J.-L. Duplan, J. Bayle, S. Lacombe, C. Thomazeau, U.S. Patent application 20050222475.
- G. T. Kokotailo, S. L. Lawton, D. H. Olson, W. M. Meier, *Nature* **272**, 437 (1978).
- K. Y. J. Zhang, P. Main, *Acta Crystallogr. A* **46**, 41 (1990).
- J. Wu, K. Leinenweber, J. C. H. Spence, M. O'Keeffe, *Nat. Mater.* **5**, 647 (2006).
- S. Brenner, L. B. McCusker, Ch. Baerlocher, *J. Appl. Cryst.* **35**, 243 (2002).
- X. D. Zou, Y. Sukharev, S. Hovmöller, *Ultramicroscopy* **52**, 436 (1993).
- X. D. Zou, A. Hovmöller, S. Hovmöller, *Ultramicroscopy* **98**, 187 (2004).
- M. A. Estermann, V. Gramlich, *J. Appl. Cryst.* **26**, 396 (1993).
- S. Hovmöller, *Ultramicroscopy* **41**, 121 (1992).
- X. D. Zou, Z. M. Mo, S. Hovmöller, X. Z. Li, K. H. Kuo, *Acta Crystallogr. A* **59**, 526 (2003).
- P. Oleynikov, X. D. Zou, S. Hovmöller, www.analitex.com/Index.html (2006).
- Ch. Baerlocher, A. Hepp, W. M. Meier, *DLS-76. Distance Least Squares Refinement Program* (Institut für Kristallographie, ETH Zurich, 1977).
- A. Corma, F. Rey, S. Valencia, J. L. Jorda, J. Rius, *Nat. Mater.* **2**, 493 (2003).
- Ch. Baerlocher, W. M. Meier, D. H. Olson, *Atlas of Zeolite Framework Types* (Elsevier, Amsterdam, 2001); and www.iza-structure.org/databases/.
- E. F. Petterson *et al.*, *J. Comput. Chem.* **25**, 1605 (2004).
- We thank H. Kessler (Université de Haute-Alsace, Mulhouse) and S. Lacombe and L. Rouleau (Institut Français du Pétrole) for providing samples of IM-5. Special thanks to L. Palatinus (EPF Lausanne) for developing the program Superflip to suit our needs. Experimental assistance from the staff at SNBL and SLS is gratefully acknowledged. This work was supported in part by the Swiss National Science Foundation, the Swedish Research Council, and Carl-Trygger's Foundation.

Supporting Online Material

www.sciencemag.org/cgi/content/full/315/5815/1113/DC1
Data files S1 and S2

22 November 2006; accepted 18 January 2007
10.1126/science.1137920

Shaping of Elastic Sheets by Prescription of Non-Euclidean Metrics

Yael Klein, Efi Efrati, Eran Sharon*

The connection between a surface's metric and its Gaussian curvature (Gauss theorem) provides the base for a shaping principle of locally growing or shrinking elastic sheets. We constructed thin gel sheets that undergo laterally nonuniform shrinkage. This differential shrinkage prescribes non-Euclidean metrics on the sheets. To minimize their elastic energy, the free sheets form three-dimensional structures that follow the imposed metric. We show how both large-scale buckling and multiscale wrinkling structures appeared, depending on the nature of possible embeddings of the prescribed metrics. We further suggest guidelines for how to generate each type of feature.

Thin sheets are common in natural and man-made structures, are shaped to a huge variety of diverse three-dimensional (3D) structures, and span many length scales (*l*). Natural slender structures, such as flowers, lichens, and marine invertebrates, attain elaborate configurations during their unconfined (free) growth. One wonders what mechanisms lead to shaping of free sheets and whether they can be implemented with artificial materials. Thin

sheets can form nontrivial 3D structures in many different ways. Confinement of flat sheets can lead to buckling (2), wrinkling (3), and crumpling (4). The construction of layered material can result in both bending (5, 6) and wrinkling (7, 8). Recent studies of wavy patterns along edges of torn plastic sheets (9–11) have shown that 3D wavy patterns can result from inplane deformations. Mathematically, a structure made of a thin sheet can be viewed as a two-dimensional (2D) surface in a 3D Euclidean space. Intrinsically, a surface is characterized by its metric, a tensor that specifies the local distances between points across the surface (12). The shape of a surface, its configuration in space, is a realization, an em-

bedding, of the metric in space. In many cases, there would be many possible embeddings of a given 2D surface (metric) in space; that is, the metric alone does not determine a configuration. To select a specific shape (a specific embedding), one needs to determine, in addition to the metric, the local curvatures on the surface (13).

We present a shape selection principle based on two main ideas: The first is Gauss theorem (Theorema Egregium), which states that the metric tensor of a surface locally determines its Gaussian curvature $K(x,y)$. The second principle, known from the study of crumpling (14–16), shell collapse (17), and wrinkling (18), states that equilibria of thin elastic sheets involve only small amount of inplane strain. Combined, these two principles lead to a novel shaping mechanism: Rather than aiming at a specific embedding, one prescribes on the sheet only a 2D metric, the “target metric” g_{tar} , one that results in a nonzero Gaussian curvature (a non-Euclidean metric). A sheet adopting a configuration (embedding) satisfying g_{tar} would have been completely free of inplane strain, that is, stretching energy. The free sheet will settle to a 3D configuration that minimizes its elastic energy. In this mechanism, the selected configuration is set by the competition between bending and stretching energies, and its metric will be close to (but

Racah Institute of Physics, Hebrew University of Jerusalem, Jerusalem, Israel.

*To whom correspondence should be addressed. E-mail: erans@vms.huji.ac.il